Multiscale Modeling of Transport and Residence Times in Nanostructured Membranes

Simón E. Albo, Linda J. Broadbelt, and Randall Q. Snurr
Dept. of Chemical and Biological Engineering and Institute for Environmental Catalysis, Northwestern University, Evanston, IL 60208

DOI 10.1002/aic.10998
Published online September 22, 2006 in Wiley InterScience (www.interscience.wiley.com).

Modeling and simulation at different scales were used to study mass transport and residence times of particles in nanostructured membranes with uniform cylindrical pores of 10–150 nm diameter and up to 5 μm long. Analytical equations of the possible mass-transport mechanisms inside the pores were used to determine that diffusion dominates over convection under the conditions of interest for selective oxidation: 700 K and pressure near atmospheric. Molecular dynamics simulations showed that surface diffusion is present only at temperatures < 700 K. Knudsen diffusion was identified as the dominant mechanism. Simulations based on its principles were performed using an ensemble of particles in a boundary-driven simulation cell, providing the average number of hits between a particle and the pore wall and the dependency of the residence time on the pore dimensions. The differences between operating a nanostructured membrane reactor in sweep-gas and pass-through modes were also investigated. © 2006 American Institute of Chemical Engineers *AIChE J,* 52: 3679–3687, 2006
Keywords: catalysis, computer simulations (MC and MD), diffusion, multiscale modeling, transport

Introduction

Mesoporous materials, which find widespread application in catalysis,[1,2] are typically used in powder or pellet form, such as in a packed-bed reactor. Robust mesoporous membrane reactors could find interesting applications and might have some advantages over pellets. For example, membrane reactors can enhance the selectivity and yield in networks of series and parallel reactions.[3] This article focuses on new, ultrauniform, inorganic, nanostructured membranes, fabricated by a combination of anodic aluminum oxidation (AAO) and atomic layer deposition (ALD).[4] The combination of these two techniques provides a flexible synthesis route to control the membrane pore diameter and the structure and composition of the pore walls.[4] AAO allows the electrochemical production of membranes with uniform cylindrical pores having diameters that range from 20 to 200 nm and lengths between 0.5 and 200 μm.[5,6] The pore diameter and wall composition can later be tailored by placing layers of oxides (such as Al_2O_3, SiO_2, and TiO_2) or other materials using ALD.[7,8] Experimental results using AAO/ALD membranes fabricated with different diameters show improved selectivity toward the desired products in the oxidative dehydrogenation of cyclohexane compared to a conventional alumina powder catalyst at the same conversion.[4]

In the oxidation of hydrocarbons, both desired and undesired reactions are exothermic and thermodynamically favored, meaning that if the reactants and products are allowed to remain in contact with the catalyst for sufficient time, total oxidation products will be obtained. Therefore, to obtain the desired partial oxidation products, thermodynamic equilibrium must be avoided by kinetically isolating the reaction products before the thermodynamically stable total oxidation products can be formed.[9] It is suspected that the short residence times that can be achieved with the nanostructured membranes synthesized by AAO and ALD play an important role in the improved selectivity results reported recently.[4] This synthesis

Correspondence concerning this article should be addressed to R. Q. Snurr at snurr@northwestern.edu.

route offers many possibilities to adjust and control the contact between reagents and catalytic sites on the walls by selecting the pore diameter, length, and composition. ALD should allow the possibility of creating asymmetric pores, such as with narrow entrances to control access and wide interiors to decrease mass-transfer resistance. The wall composition could be designed to range from hydrophobic to hydrophilic, and it may be possible to place catalytic sites or zones with precision along the length of the channels.[4]

To fully take advantage of the possibilities offered by AAO/ALD, it is necessary to understand the mass transport inside the pores so that optimal pores for a particular application can be designed. Modeling and simulation have proven useful in previous studies of transport in porous materials, with various simulation techniques being commonly used, including equilibrium molecular dynamics (EMD), nonequilibirum molecular dynamics (NEMD), and dual control volume grand canonical molecular dynamics (DCV-GCMD).[10] These techniques have been successfully applied to a variety of systems, including many studies in zeolites.[10,11] In a recent investigation of single-walled carbon nanotubes,[12] for example, pores up to 8.1 nm in diameter were studied and the authors combined molecular dynamics (MD) simulations with a theoretical approach to evaluate the viscous contribution to the transport coefficient.[13]

The present work will address pores of up to 150 nm in diameter, making it necessary to use various modeling and simulation techniques to cover the range of relevant time and length scales. The following sections will cover each of the modeling approaches separately, presenting in turn the technique, its implementation, and the results obtained. First, a review is presented of the mass-transport mechanisms of importance in pores between 10 and 150 nm. We then use analytical equations to assess the relative contributions of convection and diffusion. Following this, molecular dynamics simulations, performed to address the contribution of surface diffusion, are discussed. The results obtained up to that point will lead into the following section, where we present modeling and simulations based on Knudsen diffusion to study residence time and number and position of hits on the pore wall for a particle traveling through it.

Mass Transport Mechanisms in Nanopores

Different mass-transport mechanisms are possible inside pores, including convection, molecular diffusion, Knudsen diffusion, and surface diffusion.[14] These possible mechanisms are illustrated in Figure 1 and discussed in the following paragraphs.

Knudsen diffusion occurs when the mean free path of the molecules becomes greater than the pore diameter, so that collisions between a molecule and the pore wall occur more frequently than intermolecular collisions. Thus, this type of diffusion occurs in small pores or at low pressures. In Knudsen diffusion the collisions with the walls are assumed to be diffusive. That is, the speed and direction of the molecule leaving the surface bear no relation to the incoming values. The Knudsen diffusivity (D_K) in cylindrical pores can be calculated from kinetic theory[15]:

$$D_K = \frac{2}{3} r \sqrt{\frac{8RT}{\pi M}} \tag{1}$$

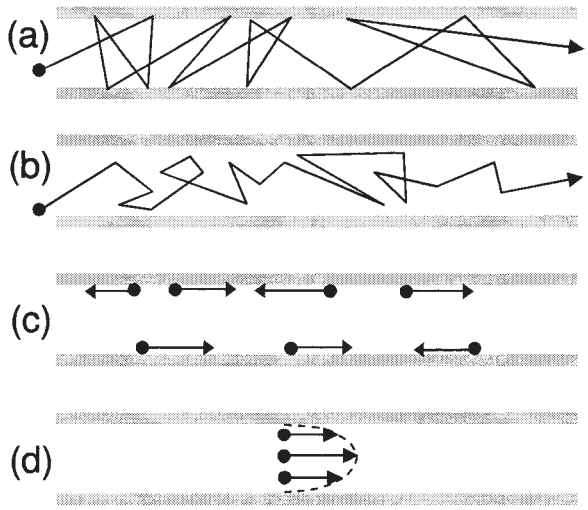

Figure 1. Mass transport mechanisms in nanopores.

(a) Knudsen diffusion, (b) molecular diffusion, (c) surface diffusion, (d) convective flow.

where r is the radius of a cylindrical pore, R is the universal gas constant, T is the absolute temperature, and M is the molecular weight of the diffusing molecule.

When the pore diameter is large relative to the mean free path, collisions among molecules will occur far more frequently than collisions between a molecule and the pore wall. Under these conditions, the influence of the wall is minor, and diffusion occurs by essentially the same mechanism as in the bulk fluid and is called molecular diffusion. The molecular diffusivity in a binary mixture (D_M) can be calculated by the Chapman–Enskog equation, which can be expressed as follows[16,17]:

$$D_M = \frac{3}{8\sqrt{2}\,\sigma_{AB}^2}\left(\frac{kT}{p}\right)\left(\frac{kT}{m^*\pi}\right)^{0.5} \tag{2}$$

where σ_{AB} is the mean molecular diameter [$\sigma_{AB} = (\sigma_A + \sigma_B)/2$], k is Boltzmann's constant, m^* is related to the molecular masses ($1/m^* = 1/m_A + 1/m_B$), and p is the pressure.

Molecular diffusion occurs when the collisions of molecules with the pore wall are unimportant compared to molecular collisions. Knudsen diffusion occurs under the opposite conditions. There will exist a transition region where both types of collisions are important. Pollard and Present[18] showed that the overall diffusivity (D_{K+M}) can then be approximated as the addition of the reciprocals of these two diffusivities:

$$\frac{1}{D_{K+M}} = \frac{1}{D_K} + \frac{1}{D_M} \tag{3}$$

This form emphasizes that resistance to the motion of molecules is serial and is caused by collisions with other gaseous molecules and by collisions with the wall.[19]

In some cases, there may be a high concentration of molecules adsorbed on the wall and they may exhibit mobility, although the mobility is substantially less than that in the vapor phase. Transport by movement of molecules over a surface is

known as surface diffusion. The fluxes through the gas phase and the adsorbed phase are to a first approximation independent and thus they are additive. The overall diffusivity will be given by the sum of the pore and surface contributions, duly weighted to take into account the difference in molecular densities between the adsorbed and vapor phases.[17] Surface diffusion is an activated process and its diffusivity ($D_{surface}$) can be described by an equation of the Arrhenius form[19]:

$$D_{surface} = D_{surface,\infty}\exp(-E_s/RT) \tag{4}$$

where $D_{surface,\infty}$ is the surface diffusion coefficient at infinite temperature and E_s is the activation energy of the process.

If there is a difference in total pressure between the ends of the pore, and under no slip conditions, there will be a bulk flow in accordance with Poiseuille's equation. This convection contribution could be represented alternatively by an equivalent Fickian diffusivity[17]:

$$D_{Poiseuille} = \frac{pr^2}{8\eta} \tag{5}$$

where p is the average pressure and η is the viscosity, which can be computed from kinetic theory. Because any such forced flow operates in parallel with the diffusive flux, it is reasonable to assume that this contribution is additive. Poiseuille flow becomes more important as the pressure and the pore diameter increase.[17]

The resultant diffusivity for a given component, incorporating the contributions from all the possible mass-transfer mechanisms (D_{total}), can be expressed as follows:

$$D_{total} = \frac{1}{\frac{1}{D_K} + \frac{1}{D_M}} + D_{Poiseuille} + KD_{surface} \tag{6}$$

where K is the dimensionless adsorption equilibrium constant expressed in terms of pore volume (moles adsorbed per unit pore volume/moles per unit volume in gas phase). Equation 6 stresses that these mass transport mechanisms could be present for any system. Their relative values will determine which of them dominates or whether their contributions are comparable in creating a transition region.

In the next section these equations are applied to the dimensions and conditions of typical AAO/ALD systems used in selective catalytic oxidation to determine the importance of the contributions of the different mass-transport mechanisms.

Convection vs. Diffusion

In this section the contributions of convection, Knudsen, and molecular diffusion to the global mass transport coefficient are compared to determine the dominant mechanism. A main objective is to identify whether the system is dominated by convection or by diffusion because this will define the behavior of the system and how the membrane should be operated. Because of the difficulty in analytically predicting surface diffusion coefficients, the role of this mechanism will be addressed in the next section through molecular dynamics simulations. We expect that surface diffusion will be relatively unimportant under the conditions for selective catalytic oxidation (SCO), which is typically carried out at elevated temperatures (600–1200 K). The system examined was typical for SCO and consisted of trace ethane in a nitrogen carrier stream with a total average pressure ranging from 1 to 2 atm and a temperature of 700 K. Using the equations presented in the previous section, the contribution of Poiseuille flow to the total mass transport coefficient is presented in Figure 2 as a function of the average pressure and pore diameter for ethane in a nitrogen carrier gas system. It shows that the major contribution to mass transport comes from the diffusive mechanisms and not from convection, especially for pores $<$50 nm in diameter, where $>$90% of the transport arises from diffusion. The relative contributions from Knudsen and molecular diffusion can be compared by calculating the Knudsen number, defined as the ratio between the mean free path and the pore diameter.[20] We find that the Knudsen mechanism dominates in the entire region, although the contribution from molecular diffusion becomes more important for the bigger pores and at the higher pressures.

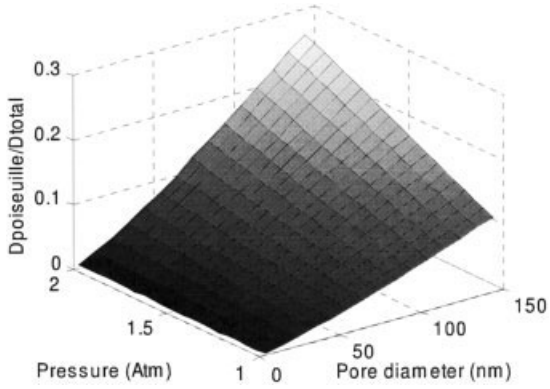

Figure 2. Convection contribution to the mass transport coefficient for ethane in a nitrogen carrier gas stream at 700 K as a function of pore diameter and average pressure.

Figure 2 provides a good general idea about the dominant mass-transport mechanism in the pores as the pore size and pressure are varied. However, it assumed no contribution from surface diffusion. Molecular dynamics simulations in the next section confirm that this assumption is valid at these conditions. The simulations may also help identify any other deviations from the mechanisms considered here that may be present in the system and could provide additional detail on the contact of reagents and catalytic sites on the pore walls.

Molecular Dynamics Simulations

Diffusivities can be calculated through molecular dynamics simulations by looking at a system in equilibrium,[11] allowing a system with a concentration gradient to relax,[21,22] applying an external field to simulate a chemical potential gradient,[21-23] or by constructing high- and low-concentration reservoirs on opposite sides of a transport zone.[22,24-26] In this work a modified version of the Music code[27] was used to perform equilibrium molecular dynamics to obtain the self-diffusivity of species inside the pores. At the low loadings of interest, it should be

expected that the self-diffusivity and Fickian diffusivities are equal.[11]

To perform molecular dynamics simulations in the pores, it is necessary to appropriately represent the alumina walls. A straightforward approach would be to fully reproduce the configuration of the walls with atomic detail. However, because of the size of the pores this would involve an impractical number of atoms and an unnecessarily expensive calculation. A simplification usually introduced is to recognize that the oxygen atoms are responsible for most of the interaction between the walls and the diffusing molecules, as was done by Fernandes and Gavalas[28] for a silica pore and by Blas et al.[29] for an alumina pore. This assumption is also extremely common in the zeolite literature.

Including only the oxygen atoms appreciably accelerates the calculations, although the number of wall atoms is still too large to achieve an efficient simulation for such large-diameter pores. Thus, further simplifications need to be introduced. Everett and Powl[30] derived the following analytical expression to represent the Lennard–Jones interaction between a molecule and two parallel semi-infinite slabs, usually called the slit-pore potential:

$$V(d_c) = \frac{2}{3}\pi n \varepsilon_{sg} \sigma_{sg}^3 \left\{ \frac{2}{15} \left[\left(\frac{\sigma_{sg}}{R_p + d_c} \right)^9 + \left(\frac{\sigma_{sg}}{R_p - d_c} \right)^9 \right] - \left[\left(\frac{\sigma_{sg}}{R_p + d_c} \right)^3 + \left(\frac{\sigma_{sg}}{R_p - d_c} \right)^3 \right] \right\} \quad (7)$$

where n is the volumetric number density of atoms in the solid, R_p is half the distance between the two parallel slabs, d_c is the distance between the particle and the midpoint between the two slabs, and σ_{sg} and ε_{sg} are the Lennard–Jones parameters for the solid–gas interactions. For larger cylindrical pores, this analytical expression can be used with R_p as the pore radius to obtain values that are very close to that of the true cylindrical potential.[28]

Equation 7 integrates the potential over a smooth and regular surface and thus the potential is not a function of the axial coordinate z, but only of the distance to the wall. As a consequence, no force is obtained in the axial direction from the particle–wall interactions when it is used alone, and the reversals in the axial velocity that are necessary to represent Knudsen diffusion are not captured. Fernandes and Gavalas[28] recognized this problem and introduced "scattering centers," that is, clusters of particles placed on the surface of the analytical potential whose number and size determine the frequency of the velocity reversals. These centers are an additive contribution to the smooth slit-pore potential and create reversals in the axial velocity.

Here we synthesized these ideas to develop a similar approach that resulted in a realistic representation of the alumina pores. An explicit layer of the surface oxygen atoms of the wall was added to the analytical potential. These atoms were added by randomly placing them without overlapping in a shell 2 Å thick with the desired internal diameter of the pore until the reported[31] density of oxygen ions in alumina, 0.052 ions/Å^3, was achieved. Ethane was treated as a sphere and the Lennard–Jones parameters used for the ethane–alumina interaction were $\varepsilon/k = 95$ K and $\sigma = 3.403$ Å as adjusted by Blas et al.[29] for the adsorption of ethane in alumina pores. The Lennard–Jones parameters for ethane–ethane interactions were $\varepsilon/k = 104.15$ K and $\sigma = 3.775$ Å.[29] A cutoff radius of 13 Å was applied for all the potentials. The interaction between the wall and an ethane molecule was compared when using a full representation of the wall and when the simplified representation (slit-pore potential plus layer of explicit atoms) was used. Excellent agreement between the potentials exerted by the two models was observed for pores $>$ 10 nm in diameter, corroborating that the slit-pore approximation is valid in large cylindrical pores and that the proposed simplified model reproduces the potential of the wall–molecule interaction very well.

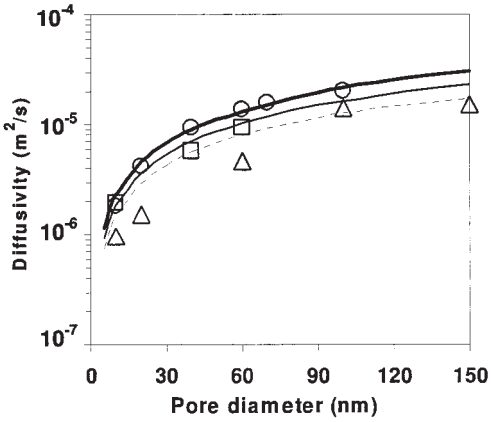

Figure 3. Self-diffusivity of ethane in alumina pores at 0.25 atm.

Lines are analytical results not including surface diffusion calculated at 700 K (—), 450 K (—), and 300 K (– – –). Points are molecular dynamics simulations results at 700 K (○), 450 K (□), and 300 K (△).

Using the simplified model, molecular dynamics (MD) simulations were performed for ethane inside alumina nanopores of diameters between 10 and 150 nm at a pressure of 0.25 atm and temperatures of 700, 450, and 300 K. The conditions of the simulations reflect a pressure that exceeds the expected typical partial pressure of the reactant and a typical elevated temperature (700 K) used to carry out SCO. Lower temperatures were also included for comparison.

In the simulations, periodic boundary conditions were applied in all directions and a simulation cell containing the compete cross section of one pore was used. The length of the simulation cell ranged from a minimum of 27 Å for the larger-pore diameters to 400 Å for the smallest diameter studied. (The cell was made longer to have enough particles in the smaller-diameter pores.) The initial configurations for the MD simulations were obtained from grand canonical Monte Carlo simulations performed at the desired temperature and pressure. The number of ethane molecules obtained ranged from 20 to 290. The MD simulations were equilibrated during 300 ps and run for 3000 ps using a time step of 0.005 ps under canonical (constant density and temperature) conditions. Constant temperature was obtained by using the Gauss thermostating method.[32] Finally, the mean square displacement was computed and Einstein's formula was used to calculate the self-diffusivity.

The self-diffusivities obtained from the MD simulations are presented in Figure 3 along with the results from the analytical equations, which include contributions only from Knudsen and

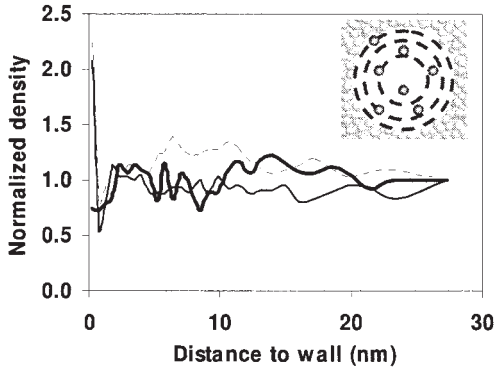

Figure 4. Radial density profile for ethane in alumina pores of 60 nm in diameter obtained from molecular dynamics simulations at 0.25 atm and 700 K (—), 450 K (—), and 300 K (– – –).

Molecules shown in the inset are not drawn to scale. Densities are normalized by dividing by the density at the center of the pore.

molecular diffusion. At 700 K the agreement between the theoretical and simulation values is excellent; this concordance indicates that surface diffusion is not present in the system under these conditions. However, as the temperature is lowered, the simulation results deviate from the theoretical results, the deviation being more accentuated for the lowest temperature studied. To explore the origin of this deviation, the radial density profiles were calculated in the simulations and the normalized densities as a function of distance to the wall for pores of 60 nm in diameter are presented in Figure 4. At 700 K the radial profile inside the pore is flat, presenting no evidence of adsorption on the pore walls and thus of surface diffusion. For the lower temperatures a significant fraction of the particles is preferentially adsorbed on the wall, indicating that surface diffusion is present in the system and that it influences the overall diffusivity.

These results lead to the conclusion that at elevated temperatures, where selective catalytic oxidation is carried out, surface diffusion is not present in the pores studied; its influence is noticeable only at much lower temperatures. Furthermore, under the range of pore sizes and conditions of interest, Knudsen diffusion is the predominant mass-transport mechanism. Based on this, in the following section we develop a simulation method to study Knudsen diffusion in these pores.

Knudsen Dynamics Simulations

Knudsen diffusion is based on two concepts: first, that a particle diffusing through the pore does not encounter other particles and collides only with the wall; and second, that these collisions are diffusive. Therefore, a simulation of a pure Knudsen regime does not require calculation of the interactions between the gas particles or between the pore wall and the gas particles; consequently, the simulations are less computationally intensive and will allow accessing longer time and length scales than molecular dynamics. Simulations following this idea have been performed for pores of different shapes[33-36] and roughness.[37-39] In all of these works the particle trajectories were considered one at a time, taking advantage of the lack of interaction among particles. Here we perform the simulation for an ensemble of particles to avoid the use of an equilibration length,[37-39] which could introduce an error in the results,[40] and also to allow the expansion of the model to study a multicomponent mixture with catalyzed reactions in the future.

It should be noted that the assumption of pure diffusive collisions between the particles and the wall might not be valid for all systems. Recent simulation studies of diffusion in carbon nanotubes have found transport diffusivities that are orders of magnitude faster than those observed in other nanoporous materials.[41,42] These high transport rates are a consequence of the reflection from the carbon nanotube being nearly specular.[12,43] In general, the nature of the collisions with the wall can be described as partly diffusive and partly specular, the relative contribution of each depending on the physical roughness of the wall and the degree of attractiveness of the wall to the fluid.[44,45] In our case, the MD simulations were performed without any assumption regarding the nature of the collisions with the walls; the good agreement of their results with Knudsen diffusion indicates that in our system the collisions can be described as purely diffusive.

The simulation cell is set up to resemble the experimental conditions where a pressure drop exists across the pores. Following the scheme of the dual control volume grand canonical molecular dynamics (DCV-GCMD) technique,[22,24,25] high- and low-pressure reservoirs are maintained on the extremes of the pore as shown in Figure 5. Because the particles do not interact with each other, the simulation is conducted by comparing the times to collide with the wall of all the particles in the system and determining the shortest time (Δt) to the next collision. Then all trajectories are advanced by Δt. The particle that collides with the wall is now assigned a new direction defined by random polar and azimuthal angles corresponding to a cosine distribution.[46] If a particle reaches one of the extremes of the simulation cell, it is deleted. All particles maintain the average speed $\bar{v}$, calculated from kinetic theory:

$$\bar{v} = \sqrt{\frac{8kT}{\pi m}} \tag{8}$$

After this procedure is repeated for a number of collisions, the simulation must be stopped to replenish the reservoirs. Because the particles are treated like hard spheres, no interactions need to be calculated and insertions or deletions are performed in each reservoir until the specified pressure is achieved. The insertions are done in random positions anywhere in the reservoir as long as there is no overlap with other particles. The newly inserted particles are each assigned a random travel direction. It was previously shown[22] that DCV-GCMD requires the addition of the streaming velocity calculated in the transport region of the simulation cell to the

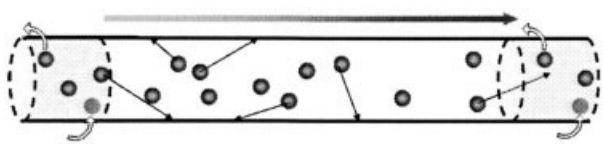

Figure 5. Boundary-driven Knudsen simulation cell.

A flow is created between the high-pressure reservoir (left) and the low-pressure reservoir (right). Insertions and deletions maintain the pressure in the reservoirs.

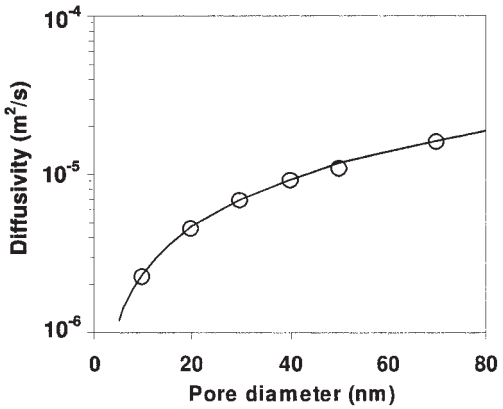

Figure 6. Ethane diffusivity from the boundary-driven Knudsen simulations (○) and theoretical values (Eq. 1) (—) at 700 K.

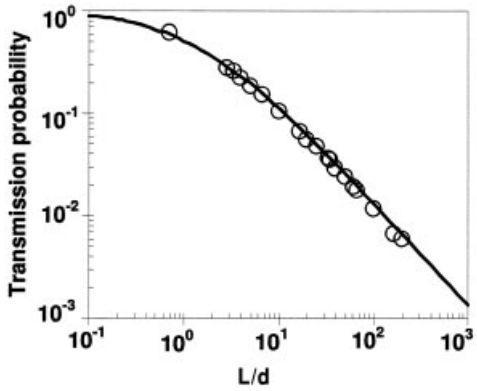

Figure 7. Transmission probability obtained from Knudsen simulations (○) and from Eq. 44 in the work of Clausing[47] (—) for pores of different aspect ratios.

particles that are inserted in the reservoirs. To incorporate this in our simulations, the streaming velocity calculated in the transport region is used as the net average velocity in the reservoirs when these are replenished, thus eliminating any discontinuity at the borders between the different regions. To minimize the time required to attain equilibrium, the simulations are started by filling the transport section with a linear concentration profile between the reservoirs. The flux is then measured and monitored at seven planes distributed throughout the transport section. The simulation is considered to achieve steady state when the fluxes in all the planes converge to the same value. The pores simulated had diameters between 10 and 70 nm and lengths from 0.05 to 5 μm. The length of the reservoirs ranged from equal to the length of the transport zone (short pores) to 10% of it (long pores). The simulated times varied from 500 to 5000 ns, with the reservoirs being replenished every 0.001 to 0.01 ns. Intervals of 0.01 to 0.1 ns were used to calculate the streaming velocity. The number of trajectories in each simulation was between 10^4 and 10^6.

From the simulations the diffusivity is calculated from Fick's law using the flux measured at the different planes and the concentration gradient. The values obtained at different pore diameters are presented in Figure 6. As expected, they agree with those predicted by Eq. 1, verifying that the simulations are performed correctly.

The Fickian diffusivity is given by the net flux in the pore; it does not, however, provide information about the residence time of the particles or about the location and number of collisions between the particles and the wall. To observe these quantities we need to study the individual trajectories of the particles. Given that the collisions are diffusive, a fraction of the particles entering the pore will exit through the same end where they entered, whereas the rest will travel through the whole length of the pore and leave it at the opposite end. The ratio of the trajectories that reach the opposite end of the pore to the number of trajectories that enter the pore is called the transmission probability. Figure 7 shows good agreement between the values of this variable obtained from the simulation and those calculated from Clausing.[47] The values of the transmission probability indicate that the particles enter the pore multiple times before reaching the opposite end of the pore, especially for larger values of the aspect ratio of pore length to pore diameter (L/d). For this reason, results for the residence times and number of hits are presented below for the two distinct trajectories: those that reach the opposite end and those that return to the initial end. In addition, it is interesting to consider a particle that is allowed to reenter the starting end as many times as needed to leave the membrane at the opposite end.

Given the potential to place catalytic sites in particular locations along the pore length by ALD and other techniques, it is of interest to determine the distribution of molecule–wall hits as a function of the distance to the entrance. This could help in choosing the sections of the pore where the catalyst should be located to optimize the contact between catalyst and reactants. This information also contributes to the identification of the differences achieved when operating the reactor in a sweep-gas mode vs. operating in a pass-through mode, where particles are removed only on the downstream side of the membrane, as depicted in Figure 8. The distributions of the average number of hits along a pore are shown in Figure 9 for a pore of aspect ratio (L/d) equal to 10. Pores of other aspect ratios have similar distributions, although the smaller the aspect ratio is, the more uniform the number of hits is along the pore length (the slopes of the distributions are smaller). When the reactor is operated in a sweep-gas mode, the relevant distributions of hits are for trajectories that return to the starting end of the pore, where they are removed by the retentate sweep gas, and for trajectories that reach the opposite end, where they are removed by the permeate sweep gas. The shapes of the two distributions are very different. When the particles return to the

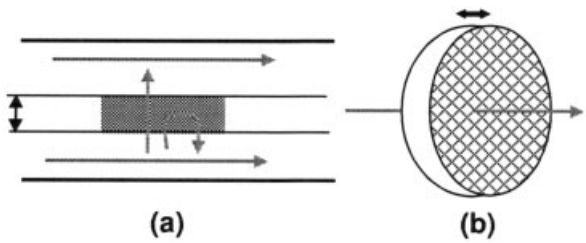

Figure 8. Possible operation modes for the membranes.

(a) Sweep-gas; (b) pass-through.

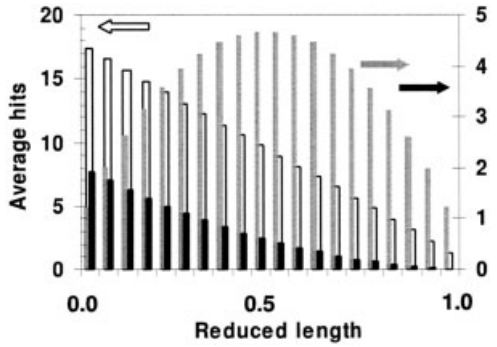

Figure 9. Average number of hits on the wall per section of a L/d = 10 pore for individual trajectories that reach the opposite end of the pore (gray bars), for those that return to the starting end of the pore (black bars), and the total average number of hits for particles recovered on the downstream end of the membrane (open bars).

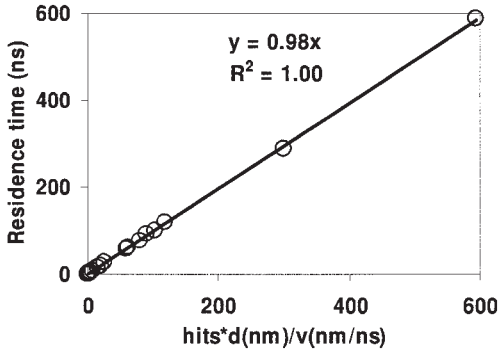

Figure 11. Residence time as a function of the number of hits, diameter of the pore, and average speed for all individual trajectories.

starting end of the pore, the majority of the hits are located near the entry point, decreasing sharply with the distance traveled inside the pore. For individual trajectories that reach the opposite end of the pore, the distribution of average hits is symmetric, with the maximum located in the center of the pore. The total average number of hits per trajectory is also important to consider for catalytic purposes. In Figure 10 this quantity is shown as a function of the aspect ratio for both types of individual trajectories. It is observed that it scales with $(L/d)^{1.79}$ for the trajectories that reach the opposite end and with $(L/d)^{0.91}$ for those trajectories returning to the initial end.

If the reactor is operated in a pass-through mode, particles are removed only when they reach the opposite end of the pore. Then, the relevant distribution of hits will account not only for the final trajectory that reached the opposite end of the pore but also for all prior trajectories that returned to the initial end of the membrane before the particle was able to reach the downstream side. The total number of hits will then be related to the transmission probability of the membrane. Figure 9 shows that the distribution of hits in this case has its maximum at the entrance of the pore and decreases linearly with the distance traveled. It can be appreciated that the total number of hits is considerably higher than that for the previously mentioned distributions. This is also observed in Figure 10, along with its scaling with $(L/d)^{1.86}$.

The residence time of particles inside the pore should be proportional to the number of hits and the average distance traveled between them and inversely proportional to the velocity of the particles. To investigate this relationship, Figure 11 shows the average residence time of individual trajectories plotted against the product of the average number of hits and the diameter of the pore, divided by the average velocity of the particles. A good fit is obtained with a slope value close to one, indicating that the average distance traveled between hits is close to the diameter of the pore. It is worth mentioning that the residence time of particles in the pores follows a distribution of values. In the case of the individual trajectories that reach the opposite end, it resembles a normal distribution but with a tail expanded to longer times, as illustrated by Figure 12a. For individual trajectories that return to the starting end of the pore, the distribution has a peak at very short times and then a tail at longer times, as shown in Figure 12b. The existence of this

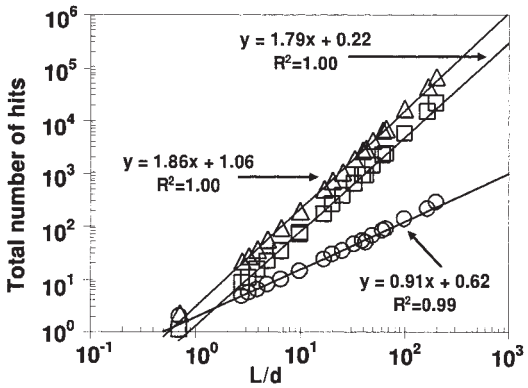

Figure 10. Average total number of hits on the wall as a function of L/d for individual trajectories that reach the opposite end of the pore (□), individual trajectories that return to the starting end of the pore (○), and the average total number of hits for a particle recovered on the downstream end of the membrane (△).

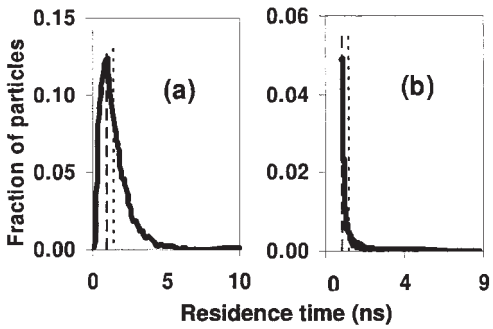

Figure 12. Residence time distribution (—), average residence time (· · ·), and most probable residence time (– – –) in a pore of L = 0.20 μm and d = 30 nm for (a) individual trajectories that reach the opposite end of the pore and (b) individual trajectories that return to the starting end of the pore.

wide distribution of residence times and number of hits should be kept in mind when designing catalytic membrane reactors based on AAO/ALD materials.

Conclusions

The combination of AAO and ALD for membrane fabrication offers the possibility of controlling the geometry of membrane reactors to regulate the residence time of particles inside the pores. In this work AAO/ALD membranes were modeled by use of a multiscale approach: analytical equations were used to determine the role of convection, molecular dynamics simulations were carried out to determine the contribution of surface diffusion, and Knudsen dynamics simulations were executed to quantify the contact between the particles traveling through the pore and the pore walls. It was found that Knudsen diffusion is the dominant mass-transport mechanism under the conditions of interest, that is, high temperature and low pressure. In this regime, it was determined that if the membrane is operated in a sweep-gas mode, particles traveling through the pore that reach the opposite end are more likely to hit the wall in the center of the pore, whereas the particles that return to the initial end of the pore will likely more frequently hit the wall near the entrance. If the membrane is operated in pass-through mode, then all particles will more frequently hit the wall near the entrance. The average number of hits per particle is higher in the pass-through mode than in the sweep-gas mode. The residence time was related to the number of hits and the velocity of the particles, revealing that the average distance traveled between hits is approximately the pore diameter. In general, the number of hits and the residence times grow with the aspect ratio (L/d) of the pore. These trends can be used as guidelines for the placement of the catalyst within the pores to optimize the contact between the catalyst and diffusing molecules.

Acknowledgments

This work was supported by the Chemical Sciences, Geosciences, and Biosciences Division, Office of Basic Energy Sciences, Office of Science, U.S. Department of Energy Grant No. DE-FG02-03ER15457. The authors thank Prof. Peter Stair for helpful discussions.

Literature Cited

1. Trong On D, Desplantier-Giscard D, Danumah C, Kaliaguine S. Perspectives in catalytic applications of mesostructured materials. *Appl Catal A Gen.* 2001;222:299-357.
2. Coronas J, Santamaria J. State-of-the-art in zeolite membrane reactors. *Top Catal.* 2004;29:29-44.
3. Tota A, Hamel C, Thomas S, Joshi M, Klose F, Seidel-Morgenstern A. Theoretical and experimental investigation of concentration and contact time effects in membrane reactors. *Chem Eng Res Des.* 2004;82: 236-244.
4. Pellin MJ, Stair PC, Xiong G, Elam JW, Birrell J, Curtiss L, George SM, Han CY, Iton L, Kung H, Kung M, Wang HH. Mesoporous catalytic membranes: Synthetic control of pore size and wall composition. *Catal Lett.* 2005;102:127-130.
5. Xiao ZL, Han CY, Welp U, Wang HH, Vlasko-Vlasov VK, Kwok WK, Miller DJ, Hiller JM, Cook RE, Willing GA, Crabtree GW. Nickel antidot arrays on anodic alumina substrates. *Appl Phys Lett.* 2002;81:2869-2871.
6. Xiao ZL, Hiller JM, Welp U, Wang HH, Kwok WK, Willing GA, Hiller JM, Cook RE, Miller DJ, Crabtree GW. Fabrication of alumina nanotubes and nanowires by etching porous alumina membranes. *Nano Lett.* 2002;2:1293-1297.
7. Elam JW, George SM. Growth of ZnO/Al_2O_3 alloy films using atomic layer deposition techniques. *Chem Mater.* 2003;15:1020-1028.
8. Elam JW, Routkevitch D, Mardilovich PP, George SM. Conformal coating on ultrahigh-aspect-ratio nanopores of anodic alumina by atomic layer deposition. *Chem Mater.* 2003;15:3507-3517.
9. Hodnett BK. *Heterogeneous Catalytic Oxidation.* New York: Wiley; 2000.
10. Keil FJ, Krishna R, Coppens MO. Modeling of diffusion in zeolites. *Rev Chem Eng.* 2000;16:71-197.
11. Theodorou DN, Snurr RQ, Bell AT. Molecular dynamics and diffusion in microporous materials. In: Alberti G, Bein T, eds. *Solid-State Supramolecular Chemistry: Two- and Three-Dimensional Inorganic Networks.* Oxford, UK: Pergamon Press; 1996;7:507-548.
12. Bhatia SK, Chen H, Sholl DS. Comparisons of diffusive and viscous contributions to transport coefficients of light gases in single-walled carbon nanotubes. *Mol Simulat.* 2005;31:643-649.
13. Bhatia SK, Nicholson D. Molecular transport in nanopores. *J Chem Phys.* 2003;119:1719-1730.
14. Cussler EL. *Diffusion, Mass Transfer in Fluid Systems.* New York: Cambridge Univ. Press; 1997.
15. Knudsen M. Die Gesetze der Molekularströmung und der inneren Riebungsströmung der Gase durch Röhren. *Ann Phys.* 1909;28:75-130.
16. Chapman S, Cowling T. *Mathematical Theory of Non-Uniform Gases.* Cambridge, UK: Cambridge Univ. Press; 1970.
17. Kärger J, Ruthven DM. *Diffusion in Zeolites and Other Microporous Solids.* New York: Wiley; 1992.
18. Pollard WG, Present RD. On gaseous self-diffusion in long capillary tubes. *Phys Rev.* 1948;73:762-774.
19. Satterfield CN. *Mass Transfer in Heterogeneous Catalysis.* Cambridge, MA: MIT Press; 1970.
20. Roy S, Raju R, Chuang HF, Cruden BA, Meyyappan M. Modeling gas flow through microchannels and nanopores. *J Appl Phys.* 2003;93: 4870-4879.
21. Maginn EJ, Bell AT, Theodorou DN. Transport diffusivities of methane in silicalite from equilibrium and nonequilibrium simulations. *J Phys Chem.* 1993;97:4173-4181.
22. Arya G, Chang HC, Maginn EJ. A critical comparison of equilibrium, non-equilibrium and boundary-driven molecular dynamics techniques for studying transport in microporous materials. *J Chem Phys.* 2001; 115:8112-8124.
23. Chempath S, Krishna R, Snurr RQ. Nonequilibrium molecular dynamics simulations of diffusion of binary mixtures containing short *n*-alkanes in faujasite. *J Phys Chem B.* 2004;108:13481-13491.
24. Heffelfinger GS, van Swol F. Diffusion in Lennard–Jones fluids using dual control volume grand canonical molecular dynamics simulation (DCV-GCMD). *J Chem Phys.* 1994;100:7548-7552.
25. MacElroy JMD. Nonequilibrium molecular dynamics simulation of diffusion and flow in thin microporous membranes. *J Chem Phys.* 1994;101:5274-5280.
26. MacElroy JMD, Suh SH. Equilibrium and nonequilibrium molecular dynamics studies of diffusion in model one-dimensional micropores. *Micropor Mesopor Mater.* 2001;48:195-202.
27. Gupta A, Chempath S, Sanborn MJ, Clark LA, Snurr RQ. Object-oriented programming paradigms for molecular modeling. *Mol Simulat.* 2003;29:29-46.
28. Fernandes NE, Gavalas GR. Molecular dynamics simulations of diffusion in mesoporous glass. *Ind Eng Chem Res.* 1999;38:723-730.
29. Blas FJ, Vega LF, Gubbins KE. Modeling new adsorbents for ethylene/ethane separations by adsorption via π-complexation. *Fluid Phase Equilib.* 1998:117-124.
30. Everett DH, Powl JC. Adsorption in slit-like and cylindrical micropores in the Henry's law region. *J Chem Soc Faraday Trans 1.*1976; 72:619-5.
31. Cascarini de Torre LE, Flores ES, Llanos JL, Bottani EJ. Gas–solid potential for N_2, O_2 and CO_2 adsorbed on graphite, amorphous carbons, Al_2O_3 and TiO_2. *Langmuir.* 1995;11:4742-4747.
32. Anderson HC. Molecular dynamics simulations at constant pressure and/or temperature. *J Chem Phys.* 1980;72:2384-2393.
33. Davis DH. Monte Carlo calculation of molecular flow rates through a cylindrical elbow and pipes of other shapes. *J Appl Phys.* 1960;31: 1169-1176.
34. Evans JW, Abbasi MH, Sarin A. A Monte Carlo simulation of the diffusion of gases in porous solids. *J Chem Phys.* 1980;72:2967-2973.

35. Nakano Y, Iwamoto S, Akai K, Evans JW. Collision frequencies of gas molecules with pore walls. *Chem Eng Commun.* 1985;42:129-138.
36. Nakano Y, Iwamoto S, Yoshinaga I, Evans JW. The effect of pore necking on Knudsen diffusivity and collision frequency of gas molecules with pore walls. *Chem Eng Sci.* 1987;42:1577-1583.
37. Malek K, Coppens MO. Effects of surface roughness on self- and transport diffusion in porous media in the Knudsen regime. *Phys Rev Lett.* 2001;87:1255051-1255054.
38. Malek K, Coppens MO. Pore roughness effects on self- and transport diffusion in nanoporous materials. *Colloid Surf A.* 2002;206:335-348.
39. Malek K, Coppens MO. Knudsen self- and Fickian diffusion in rough nanoporous media. *J Chem Phys.* 2003;119:2801-2811.
40. Russ S, Zschiegner S, Bunde A, Kärger J. Lambert diffusion in porous media in the Knudsen regime: Equivalence of self-diffusion and transport diffusion. *Phys Rev E.* 2005;72:0301011-0301014.
41. Chen H, Sholl DS. Predictions of selectivity and flux for CH_4/H_2 separations using single walled carbon nanotubes as membranes. *J Membr Sci.* 2006;269:152-160.
42. Skoulidas AI, Ackerman DM, Johnson JK, Sholl DS. Rapid transport of gases in carbon nanotubes. *Phys Rev Lett.* 2002;89:1859011-1859014.
43. Chen H, Sholl DS. Rapid diffusion of CH_4/H_2 mixtures in single-walled carbon nanotubes. *J Am Chem Soc.* 2004;126:7778-7779.
44. Arya G, Chang HC, Maginn EJ. Molecular simulations of Knudsen wall-slip: Effect of wall morphology. *Mol Simulat.* 2003;29:697-709.
45. Arya G, Chang HC, Maginn EJ. Knudsen diffusivity of a hard sphere in a rough slit pore. *Phys Rev Lett.* 2003;91:0261021-0261024.
46. Greenwood J. The correct and incorrect generation of a cosine distribution of scattered particles for Monte-Carlo modelling of vacuum systems. *Vacuum.* 2002;67:217-222.
47. Clausing P. The flow of highly rarefied gases through tubes of arbitrary length. *Ann Phys.* 1932;5:961-989.

Manuscript received Mar. 23, 2006, and revision received July 8, 2006.